Research Article Vol. 4, No. 9 / September 2017 / Optica 1052

optica

Demonstration of an optical-coherence converter

Chukwuemeka Okoro,[1,†,*] H. Esat Kondakci,[2,†] Ayman F. Abouraddy,[2] and Kimani C. Toussaint, Jr.[3]

[1]Department of Electrical and Computer Engineering, University of Illinois at Urbana–Champaign, Urbana, Illinois 61801, USA
[2]CREOL, The College of Optics & Photonics, University of Central Florida, Orlando, Florida 32816, USA
[3]Department of Mechanical Science and Engineering, University of Illinois at Urbana–Champaign, Urbana, Illinois 61801, USA
*Corresponding author: okoro2@illinois.edu

Received 12 June 2017; revised 19 July 2017; accepted 4 August 2017 (Doc. ID 297889); published 30 August 2017

Studying the coherence of an optical field is typically compartmentalized with respect to its different physical degrees of freedom (DoFs)—spatial, temporal, and polarization. Although this traditional approach succeeds when the DoFs are uncoupled, it fails at capturing key features of the field's coherence if the DOFs are indeed correlated—a situation that arises often. By viewing coherence as a "resource" that can be shared among the DoFs, it becomes possible to convert the entropy associated with the fluctuations in one DoF to another DoF that is initially fluctuation-free. Here, we verify experimentally that coherence can indeed be reversibly exchanged—without loss of energy—between polarization and the spatial DoF of a partially coherent field. Starting from a linearly polarized spatially incoherent field—one that produces no spatial interference fringes—we obtain a spatially coherent field that is unpolarized. By reallocating the entropy to polarization, the field becomes invariant with regard to the action of a polarization scrambler, thus suggesting a strategy for avoiding the deleterious effects of a randomizing system on a DoF of the optical field. © 2017 Optical Society of America

OCIS codes: (030.0030) Coherence and statistical optics; (030.1640) Coherence; (260.3160) Interference; (260.0260) Physical optics.

https://doi.org/10.1364/OPTICA.4.001052

1. INTRODUCTION

Optical coherence is evaluated by assessing the correlations between field fluctuations at different points in space and time [1]. When multiple degrees of freedom (DoFs) of an optical field—spatial, temporal, and polarization—are relevant, the coherence of each DoF is typically studied separately. For example, spatial coherence is evaluated via double-slit interference [2], temporal coherence through two-path (e.g., Michelson) interference [3], and polarization coherence by measuring the Stokes parameters [4]. Although this traditional approach succeeds when the DoFs are uncoupled, it fails at capturing key features of the field coherence if they are correlated [5,6].

Here we show that coherence can be viewed as a "resource" that can be reversibly converted from one DoF of the field to another. We demonstrate experimentally the reversible and energy-conserving (unitary) conversion of coherence between the spatial and polarization DoFs of an optical field. Starting from a linearly polarized field having *no spatial coherence* (a complete lack of double-slit interference visibility), we convert the field without filtering or loss of energy into one that displays spatial coherence (high-visibility interference fringes) but is *unpolarized*. The optical arrangement we describe engenders an internal reorganization of the field energy that leads to a migration of the entropy associated with the statistical fluctuations from one DoF (spatial) to another (polarization). This coherency conversion is confirmed by measuring the full 4×4 coherency matrix that provides a complete description of two-point vector-field coherence via "optical coherency matrix tomography" (OCmT) [7,8]. The tomographic measurement of coherence is carried out at different stages in the experimental setup to confirm the transformations involved in the coherence conversion process. As an application to highlight the usefulness of reallocating the entropy from one DoF of the field to another, we show that the field can be reconfigured to be invariant under the impact of a depolarizer or polarization scrambler that transforms any input polarization to unpolarized light. By transferring all the field entropy into polarization, the polarization scrambler cannot further increase the polarization entropy, which thus emerges unchanged. Since the coherence conversion procedure is reversible and no energy is lost, the field may be reversed to its original fully polarized configuration after traversing the polarization scrambler.

The paper first briefly reviews the matrix approach to quantifying optical coherence for a single DoF and multiple DoFs. Second, we describe the concept of an optical-coherence converter, a system that reversibly transforms coherence—viewed as a resource—from one DoF of a field to another without loss of energy. Starting from a field with one coherent DoF and another incoherent DoF, we reversibly convert the field such that the former DoF becomes incoherent and the latter coherent. Third, we present the experimental arrangement used in confirming these predictions and the measurement scheme to identify multi-DoF beam coherence. Finally, we demonstrate the invariance of a field with respect to a polarization scrambler before presenting our conclusions.

2. MULTI-DoF COHERENCE

A. Polarization Coherence and Spatial Coherence

Partial polarization is described by a polarization coherency matrix $\boldsymbol{G}_\mathrm{p} = \left(\begin{smallmatrix} G^{\mathrm{HH}} & G^{\mathrm{HV}} \\ G^{\mathrm{VH}} & G^{\mathrm{VV}} \end{smallmatrix}\right)$, where H and V identify the horizontal and vertical polarization components, respectively, $G^{ij} = \langle E^i (E^j)^* \rangle$, $i, j = \mathrm{H}, \mathrm{V}$, and $\langle \cdot \rangle$ is an ensemble average [9]. Here, $\boldsymbol{G}_\mathrm{p}$ is Hermitian ($\boldsymbol{G}_\mathrm{p}^\dagger = \boldsymbol{G}_\mathrm{p}$), semi-positive, normalized such that $G^{\mathrm{HH}} + G^{\mathrm{VV}} = 1$, G^{HH} and G^{VV} are the contributions of H and V to the total power, respectively, and G^{HV} is their normalized correlation. The degree of polarization is $D_\mathrm{p} = |\lambda_\mathrm{H} - \lambda_\mathrm{V}|$, where λ_H and λ_V are the eigenvalues of $\boldsymbol{G}_\mathrm{p}$ [10]. Spatial coherence can be similarly described via a spatial coherency matrix for points $\vec{a}$ and $\vec{b}$, $\boldsymbol{G}_\mathrm{s} = \left(\begin{smallmatrix} G_{aa} & G_{ab} \\ G_{ba} & G_{bb} \end{smallmatrix}\right)$, where $G_{kl} = \langle E_k E_l^* \rangle$, $k, l = a, b$. The properties of $\boldsymbol{G}_\mathrm{s}$ are similar to those of $\boldsymbol{G}_\mathrm{p}$. The visibility of the interference fringes observed by superposing the fields from $\vec{a}$ and $\vec{b}$ is $V = 2|G_{ab}|$. Alternatively, the degree of spatial coherence $D_\mathrm{s} = |\lambda_a - \lambda_b|$ represents the *maximum* visibility obtained after equalizing the amplitudes at $\vec{a}$ and $\vec{b}$, where λ_a and λ_b are the eigenvalues of $\boldsymbol{G}_\mathrm{s}$ [2,11].

A DoF represented by a 2×2 coherency matrix carries up to 1 bit of entropy; e.g., the polarization entropy is $S_\mathrm{p} = -\lambda_\mathrm{H} \log_2 \lambda_\mathrm{H} - \lambda_\mathrm{V} \log_2 \lambda_\mathrm{V}$, where $0 \le S_\mathrm{p} \le 1$. The zero-entropy state $S_\mathrm{p} = 0$ corresponds to a fully polarized field (no statistical fluctuations), whereas the maximal-entropy state $S_\mathrm{p} = 1$ corresponds to an unpolarized field (maximal fluctuations) [12]; similarly for the spatial DoF based on $\boldsymbol{G}_\mathrm{s}$. Entropy so defined is a *unitary invariant* of the field DoF: it cannot be changed by applying lossless deterministic optical transformations.

B. Joint Polarization and Spatial Coherence Formalism

Evaluating $\boldsymbol{G}_\mathrm{p}$ and $\boldsymbol{G}_\mathrm{s}$ is *not* sufficient to completely identify the coherence of a vector field in which the polarization and spatial DoFS are potentially correlated. A 4×4 coherency matrix $\boldsymbol{G}$ is necessary to capture the full vector-field coherence [6,13],

$$\boldsymbol{G} = \begin{pmatrix} G_{aa}^{\mathrm{HH}} & G_{aa}^{\mathrm{HV}} & G_{ab}^{\mathrm{HH}} & G_{ab}^{\mathrm{HV}} \\ G_{aa}^{\mathrm{VH}} & G_{aa}^{\mathrm{VV}} & G_{ab}^{\mathrm{VH}} & G_{ab}^{\mathrm{VV}} \\ G_{ba}^{\mathrm{HH}} & G_{ba}^{\mathrm{HV}} & G_{bb}^{\mathrm{HH}} & G_{bb}^{\mathrm{HV}} \\ G_{ba}^{\mathrm{VH}} & G_{ba}^{\mathrm{VV}} & G_{bb}^{\mathrm{VH}} & G_{bb}^{\mathrm{VV}} \end{pmatrix}, \tag{1}$$

where $G_{kl}^{ij} = \langle E_k^i (E_l^j)^* \rangle$, $i, j = \mathrm{H}, \mathrm{V}$, and $k, l = a, b$. The matrix $\boldsymbol{G}$ is Hermitian positive semi-definite and normalized such that $\mathrm{Tr}\{\boldsymbol{G}\} = 1$ ("Tr" is the matrix trace). The diagonal elements are the power fractions from the mutually exclusive contributions: G_{aa}^{HH} and G_{aa}^{VV} are the H and V components at $\vec{a}$, respectively, and G_{bb}^{HH} and G_{bb}^{VV} are those at $\vec{b}$. The off-diagonal elements are normalized correlations between field components. The double-slit visibility observed when overlapping the fields from $\vec{a}$ and $\vec{b}$ is $V = 2|G_{ab}^{\mathrm{HH}} + G_{ab}^{\mathrm{VV}}|$ [14]. Crucially, V is *not a unitary invariant* of the field [15,16], and reversible optical transformations that span the spatial and polarization DoFs can increase V [17,18].

Each *physically independent* DoF (spatial and polarization) carries 1 bit of entropy, so the vector field now carries 2 bits of entropy: $S = -\lambda_{a\mathrm{H}} \log_2 \lambda_{a\mathrm{H}} - \lambda_{a\mathrm{V}} \log_2 \lambda_{a\mathrm{V}} - \lambda_{b\mathrm{H}} \log_2 \lambda_{b\mathrm{H}} - \lambda_{b\mathrm{V}} \log_2 \lambda_{b\mathrm{V}}$, where $0 \le S \le 2$ and $\{\lambda\} = \{\lambda_{a\mathrm{H}}, \lambda_{a\mathrm{V}}, \lambda_{b\mathrm{H}}, \lambda_{b\mathrm{V}}\}$ are the real positive eigenvalues of $\boldsymbol{G}$. The zero-entropy state $S = 0$ corresponds to a fully polarized *and* spatially coherent field (no statistical fluctuations in either DoF and $\{\lambda\} = \{1, 0, 0, 0\}$), whereas the maximal-entropy state $S = 2$ corresponds to an unpolarized spatially incoherent field (maximal fluctuations in both DoFs and $\{\lambda\} = \frac{1}{4}\{1, 1, 1, 1\}$).

3. CONCEPT OF OPTICAL COHERENCY CONVERSION

In general, $S \le S_\mathrm{p} + S_\mathrm{s}$, with equality achieved only when the two DoFs are independent, in which case $\boldsymbol{G}$ can be written in separable form $\boldsymbol{G} = \boldsymbol{G}_\mathrm{s} \otimes \boldsymbol{G}_\mathrm{p}$. In general, S_s and S_p are obtained from the 2×2 "reduced" spatial and polarization coherency matrices

$$\boldsymbol{G}_\mathrm{s}^{(\mathrm{r})} = \begin{pmatrix} G_{aa}^{\mathrm{HH}} + G_{aa}^{\mathrm{VV}} & G_{ab}^{\mathrm{HH}} + G_{ab}^{\mathrm{VV}} \\ G_{ba}^{\mathrm{HH}} + G_{ba}^{\mathrm{VV}} & G_{bb}^{\mathrm{HH}} + G_{bb}^{\mathrm{VV}} \end{pmatrix},$$
$$\boldsymbol{G}_\mathrm{p}^{(\mathrm{r})} = \begin{pmatrix} G_{aa}^{\mathrm{HH}} + G_{bb}^{\mathrm{HH}} & G_{aa}^{\mathrm{HV}} + G_{bb}^{\mathrm{HV}} \\ G_{aa}^{\mathrm{VH}} + G_{aa}^{\mathrm{VH}} & G_{aa}^{\mathrm{VV}} + G_{bb}^{\mathrm{VV}} \end{pmatrix}, \tag{2}$$

which are obtained from $\boldsymbol{G}$ by a "partial trace" [19], that is, by tracing over one DoF [6,7].

The concept of an optical-coherence converter is illustrated in Fig. 1(a). Consider the case when the field carries 1 bit of entropy ($S = 1$) and the DoFs are independent ($S = S_\mathrm{p} + S_\mathrm{s}$), in which case a single DoF can accommodate this entropy. The field may be maximally *incoherent* but polarized ($S_\mathrm{s} = 1$ and $S_\mathrm{p} = 0$), whereupon no interference fringes can be observed [Fig. 1(b)]. Alternatively, the field may be spatially coherent but *un* polarized ($S_\mathrm{s} = 0$ and $S_\mathrm{p} = 1$), in which case full-visibility fringes can be observed [Fig. 1(c)]. We demonstrate here that an optical field can be *reversibly* transformed from the former configuration to the latter without loss of energy, thus *converting* coherence from one DoF (polarization) to the other (spatial). Throughout the procedure, S remains constant; that is, no uncertainty is added or removed from the field, only an internal reorganization of the field engendered by a unitary transformation confines the statistical fluctuations to one DoF while freeing the other from uncertainty. We call such a system a "coherence converter."

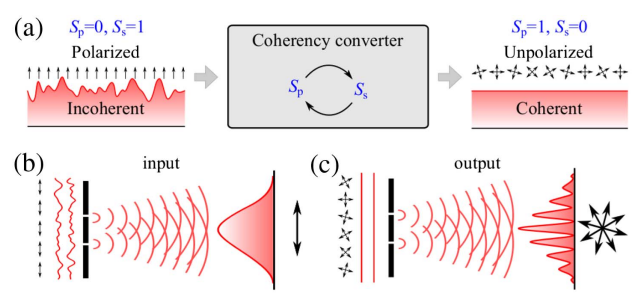

Fig. 1. Concept of an optical-coherence converter. (a) Starting with a polarized but spatially incoherent field ($S_\mathrm{p} = 0$ and $S_\mathrm{s} = 1$, $S = S_\mathrm{p} + S_\mathrm{s} = 1$), coherence is converted from polarization to the spatial DoF, thereby yielding an unpolarized but spatially coherent field ($S_\mathrm{p} = 1$ and $S_\mathrm{s} = 0$) but without introducing further fluctuations (fixed total entropy $S = 1$). The device thus converts the statistical fluctuations (and the attendant entropy) from one DoF to the other. (b) When a polarized but spatially incoherent field is incident on a double slit, no interference fringes are observed. (c) After converting coherence from polarization to the spatial DoF, high-visibility (but unpolarized) interference fringes appear.

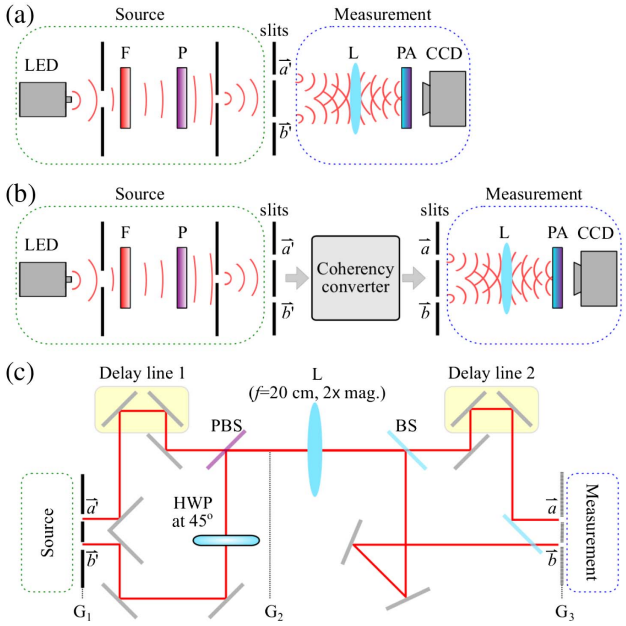

Fig. 2. (a) Schematic depicting the input field preparation (source) and characterization (measurement). The field at points $\vec{a}'$ and $\vec{b}'$ is spatially incoherent but fully polarized (scalar). F, filter; P, polarizer; L, lens; PA, polarization analyzer; CCD, charge-coupled device camera. (b) A coherency converter maps the spatially incoherent but polarized field at $\vec{a}'$ and $\vec{b}'$ to a spatially coherent but unpolarized field at $\vec{a}$ and $\vec{b}$. (c) Schematic of the optical setup for the coherence-converter. A biconvex lens (L: $f = 20$ cm) images $\vec{a}'$ and $\vec{b}'$ to $\vec{a}$ and $\vec{b}$, respectively, with 2× magnification. The delay lines enable matching pairs of paths within the source temporal coherence length. HWP, half-wave plate; PBS, polarizing beam splitter; BS, beam splitter. The planes at which the coherency matrices $\boldsymbol{G}_1$, $\boldsymbol{G}_2$, and $\boldsymbol{G}_3$ are reconstructed are marked.

The optical arrangement we propose to convert coherency between the spatial and polarization DoFs is depicted in Fig. 2. We start from two points $\vec{a}'$ and $\vec{b}'$ of equal intensity in a spatially *in* coherent H-polarized field (the fields are mutually incoherent or statistically independent), which thus produce no interference fringes. The polarization at $\vec{b}'$ is rotated to become orthogonal to that at $\vec{a}'$ (H → V) before combining the fields at a polarizing beam splitter (PBS), which yields an *un* polarized field. We then split the field into two points $\vec{a}$ and $\vec{b}$ using a *non* polarizing beam splitter, which creates two copies of the field that can demonstrate high-visibility interference fringes. We proceed now to present the measurements at each step of this coherency-conversion process.

4. SOURCE CHARACTERIZATION

The optical field we study is extracted from a broadband, unpolarized LED (center wavelength 850 nm, 30 nm FWHM bandwidth; Thorlabs M850L3 IR). The field is spectrally filtered (10 nm FWHM), polarized along H, and spatially filtered through a 100 μm wide slit placed at a distance of 180 mm from the source. The "input" plane that includes the points $\vec{a}'$ and $\vec{b}'$ (each defined by a 100 μm wide slit) is located 420 mm away from the slit [the source in Fig. 2(a)]. We first confirm that the field is spatially coherent within $\vec{a}'$ and $\vec{b}'$ separately (i.e., the spatial coherence width of the field, estimated to be ∼1 mm, is larger than the slit width). This is accomplished using a narrow pair of slits (50 μm wide separated by $\Delta = 150$ μm) at

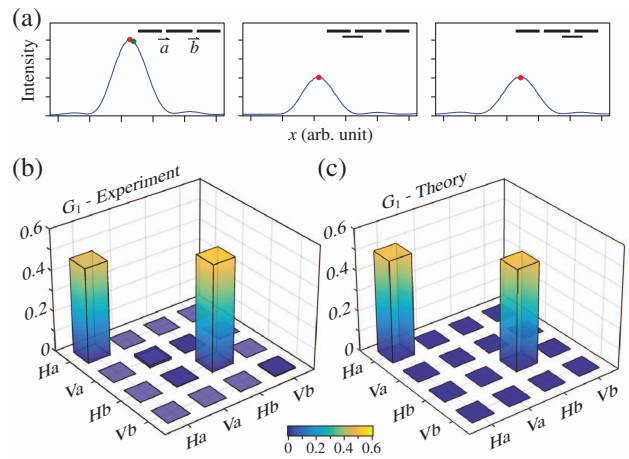

Fig. 3. (a) Four measurements required to reconstruct the spatial coherence matrix $\boldsymbol{G}_S$ for a scalar field at $\vec{a}$ and $\vec{b}$. The intensity pattern is recorded with both slits open (left), and two measurements are made: the intensity on the optical axis (red dot) and at the location midway along the first expected fringe location calculated from the slit separation (green dot). No fringes are observed here since the field is spatially incoherent. Next, the intensity on the optical axis is recorded when $\vec{a}$ (left) and $\vec{b}$ (right) are blocked (the red dots; see Refs. [7,8] for details). (b) Plot depicting graphically the real parts of the elements of the spatial-polarization coherency matrix $\boldsymbol{G}_1$ for the source plane as reconstructed from OCmT that utilizes the measurements in (a) when carried out in conjunction with polarization measurements. (c) Plot graphically depicting the elements of the theoretically expected coherency matrix $\boldsymbol{G} = \frac{1}{2}\mathrm{diag}\{1, 0, 1, 0\}$, corresponding to a scalar H-polarized field that is spatially incoherent [Eq. (3)].

either $\vec{a}'$ or $\vec{b}'$ and observing the double-slit interference on a CCD camera (Hamamatsu 1394) at a distance of $d = 200$ mm away. High-visibility fringes ($V = 0.98$) are observed separated by $\lambda d/\Delta \approx 1170$ μm. Next, we superpose the fields from $\vec{a}'$ and $\vec{b}'$ ["measurement" in Fig. 2(a)] and observe no interference fringes [Fig. 3(a)], confirming that the two points are separated by more than the field coherence width. We have thus confirmed the relationship between the two length scales involved: the sizes of the locations at $\vec{a}'$ and $\vec{b}'$ (100 μm) are smaller than the coherence width, and the separation between them (10 mm) is larger. The field that we start from is linearly polarized (scalar) but spatially incoherent, thus $\boldsymbol{G}$ has the form

$$\boldsymbol{G}_1 = \frac{1}{2}\begin{pmatrix} 1 & 0 & 0 & 0 \\ 0 & 0 & 0 & 0 \\ 0 & 0 & 1 & 0 \\ 0 & 0 & 0 & 0 \end{pmatrix} = \frac{1}{2}\begin{pmatrix} 1 & 0 \\ 0 & 1 \end{pmatrix}_{\mathrm{s}} \otimes \begin{pmatrix} 1 & 0 \\ 0 & 0 \end{pmatrix}_{\mathrm{p}}, \quad \textbf{(3)}$$

where the subscripts "s" and "p" refer to the spatial and polarization DoFs, respectively, and the notation diag{·} identifies a diagonal matrix with the entries along the diagonal listed between the curly brackets.

To fully characterize the field coherence across the spatial and polarization DoFs, we measure $\boldsymbol{G}_1$ via OCmT [7,8], which requires 16 measurements to reconstruct $\boldsymbol{G}_1$. Since four polarization projections are required to identify $\boldsymbol{G}_{\mathrm{p}}$ and four spatial projections are required to determine $\boldsymbol{G}_{\mathrm{s}}$ for a scalar field, 4×4 linearly independent combinations of these spatial and polarization projections are necessary to reconstruct $\boldsymbol{G}$ subject to the constraints of Hermiticity, semi-positiveness, and unity trace. These measurements are in one-to-one correspondence to those required

to reconstruct a two-qubit density matrix in quantum mechanics, a process known as "quantum state tomography" [20–22]. Carrying out these optical measurements (see [8] for details), $\boldsymbol{G}_1$ is reconstructed [Fig. 3(b)] and found to be in good agreement with the theoretical expectation [Fig. 3(c)], with the remaining slight deviations attributable to unequal powers at $\vec{a}'$ and $\vec{b}'$.

The measured coherency matrix $\boldsymbol{G}_1$ in the $(\vec{a}', \vec{b}')$ plane yields $S = 1.001$, and the reduced spatial and polarization coherency matrices $\boldsymbol{G}_{\mathrm{s}}^{(\mathrm{r})}$ and $\boldsymbol{G}_{\mathrm{p}}^{(\mathrm{r})}$ obtained from $\boldsymbol{G}$ yield $S_{\mathrm{s}} = 0.991$ and $S_{\mathrm{p}} = 0.037$, respectively. The field entropy is thus associated with the spatial DoF and *not* polarization, resulting in an absence of interference fringes [Fig. 3(a)]. The lack of interference fringes is consistent with the fact that all measures of spatial coherence or double-slit interference fringes for a *vector field* rely on the cross-correlation matrix [14] or beam-coherence matrix [23], $\boldsymbol{G}_{ab} = \begin{pmatrix} G_{ab}^{\mathrm{HH}} & G_{ab}^{\mathrm{HV}} \\ G_{ab}^{\mathrm{VH}} & G_{ab}^{\mathrm{VV}} \end{pmatrix}$, which is the top-right 2×2 block of the coherency matrix $\boldsymbol{G}$. For example, the degree of coherence proposed by Wolf [14], the degree of electromagnetic coherence [15,16], the complex degree of mutual polarization [24], the visibility predicted through a generalized form of the Fresnel–Arago law [25], or the maximal visibility obtainable through local unitary transformations [17,18] all predict that the observed visibility will be zero if all the entries in $\boldsymbol{G}_{ab}$ are zero. Because the measured and theoretically expected $\boldsymbol{G}_1$ has all zero entries in the $\boldsymbol{G}_{ab}$ block, it follows that interference fringes do not form. We proceed to show that interference fringes nevertheless appear once the coherence has been *reversibly converted* from polarization to the spatial DoF.

5. CONVERTING COHERENCE FROM POLARIZATION TO SPACE

Converting the coherence reversibly from polarization to the spatial DoF entails maximizing the polarization entropy S_{p} and minimizing the spatial entropy S_{s} at *fixed* total entropy S. A half-wave plate (HWP) placed after $\vec{b}'$ rotates the polarization $\mathrm{H} \to \mathrm{V}$, resulting in a new coherency matrix $\boldsymbol{G} = \frac{1}{2}\mathrm{diag}\{1, 0, 0, 1\}$. The fields from $\vec{a}'$ and $\vec{b}'$ are then directed by mirrors to the two input ports of a PBS (Thorlabs CM1-PBS252), where the V component is transmitted and H is reflected [Fig. 4(a)]. Consequently, the H and V components overlap in the same output port at $\vec{a}''$ (minimal power in the other port $\vec{b}''$). Note that a PBS is a reversible device: when the two output fields reverse their direction and return to the PBS, the input fields are reconstituted. The field is now unpolarized, which we confirm by registering a flat Malus curve and comparing it to the sinusoidal Malus curve produced by the linearly polarized input fields [Fig. 4(b)]. That is, each incident field on the PBS is linearly polarized, whereas their superposition at the output—with the initial optical power now concentrated in a single path—is randomly polarized. The coherency matrix $\boldsymbol{G}_2$ at $\vec{a}''$ and $\vec{b}''$ is reconstructed via OCmT [Fig. 4(c)] and is found to be in good agreement with the expected form [Fig. 4(d)]:

$$\boldsymbol{G}_2 = \frac{1}{2}\begin{pmatrix} 1 & 0 & 0 & 0 \\ 0 & 1 & 0 & 0 \\ 0 & 0 & 0 & 0 \\ 0 & 0 & 0 & 0 \end{pmatrix} = \begin{pmatrix} 1 & 0 \\ 0 & 0 \end{pmatrix}_{\mathrm{s}} \otimes \frac{1}{2}\begin{pmatrix} 1 & 0 \\ 0 & 1 \end{pmatrix}_{\mathrm{p}}. \quad (4)$$

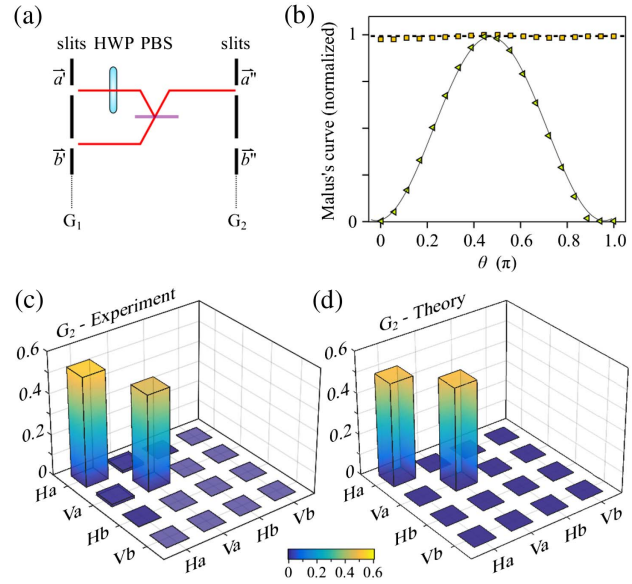

Fig. 4. (a) Schematic for the setup to combine two linearly polarized fields from $\vec{a}'$ and $\vec{b}'$ that are statistically independent or spatially incoherent ($S_{\mathrm{p}} = 0$ and $S_{\mathrm{s}} = 1$) into $\vec{a}''$ and $\vec{b}''$ whereupon the field becomes unpolarized but spatially coherent ($S_{\mathrm{p}} = 1$ and $S_{\mathrm{s}} = 0$), without loss of power or increase in total entropy $S = 1$. HWP, half-wave plate rotated to implement the transformation $\mathrm{H} \to \mathrm{V}$; PBS, polarizing beam splitter. (b) Malus curves for fields at the two input ports of the PBS highlight the linear polarization (one orthogonal to the other) and that for the field at the output port highlights its random polarization. The dashed and continuous lines are the flat and sinusoidal curves associated with unpolarized and V-polarized light, respectively. (c) Graphical depiction of the elements of the full coherency matrix $\boldsymbol{G}_2$ is obtained experimentally and (d) expected theoretically.

It is important to note that the two spatial modes derived from $\vec{a}'$ and $\vec{b}'$ completely overlap in a single mode after the PBS. This is confirmed by placing double slits separated by 150 μm right after the PBS and observing high-visibility interference fringes (thus eliminating the possibility of incoherence due to reduced spatial overlap [26]).

From the reconstructed $\boldsymbol{G}_2$ in the $(\vec{a}'', \vec{b}'')$ plane, the total entropy is $S = 0.997$, but the new values of entropy for the spatial and polarization DoFs are $S_{\mathrm{s}} = 0.001$ and $S_{\mathrm{p}} = 0.996$, respectively. *The entropy has now been converted between the two DoFs*. To observe interference fringes, the randomly polarized field at $\vec{a}''$ is split symmetrically into two halves by a 50:50 *non*-polarizing beam splitter to points $\vec{a}$ and $\vec{b}$ [Fig. 5(a)], which can then be overlapped to produce high-visibility fringes. This step does not change the values of S, S_{s}, or S_{p}. The $(\vec{a}, \vec{b})$ plane is the image plane relayed from the $(\vec{a}', \vec{b}')$ plane by a lens [Fig. 2(c)]. The coherency matrix $\boldsymbol{G}_3$ in this plane is

$$\boldsymbol{G}_3 = \frac{1}{4}\begin{pmatrix} 1 & 0 & 1 & 0 \\ 0 & 1 & 0 & 1 \\ 1 & 0 & 1 & 0 \\ 0 & 1 & 0 & 1 \end{pmatrix} = \frac{1}{2}\begin{pmatrix} 1 & 1 \\ 1 & 1 \end{pmatrix}_{\mathrm{s}} \otimes \frac{1}{2}\begin{pmatrix} 1 & 0 \\ 0 & 1 \end{pmatrix}_{\mathrm{p}}. \quad (5)$$

The measured $\boldsymbol{G}_3$ reconstructed via OCmT [Fig. 5(b)] is in good agreement with the theoretical expectation [Fig. 5(c)].

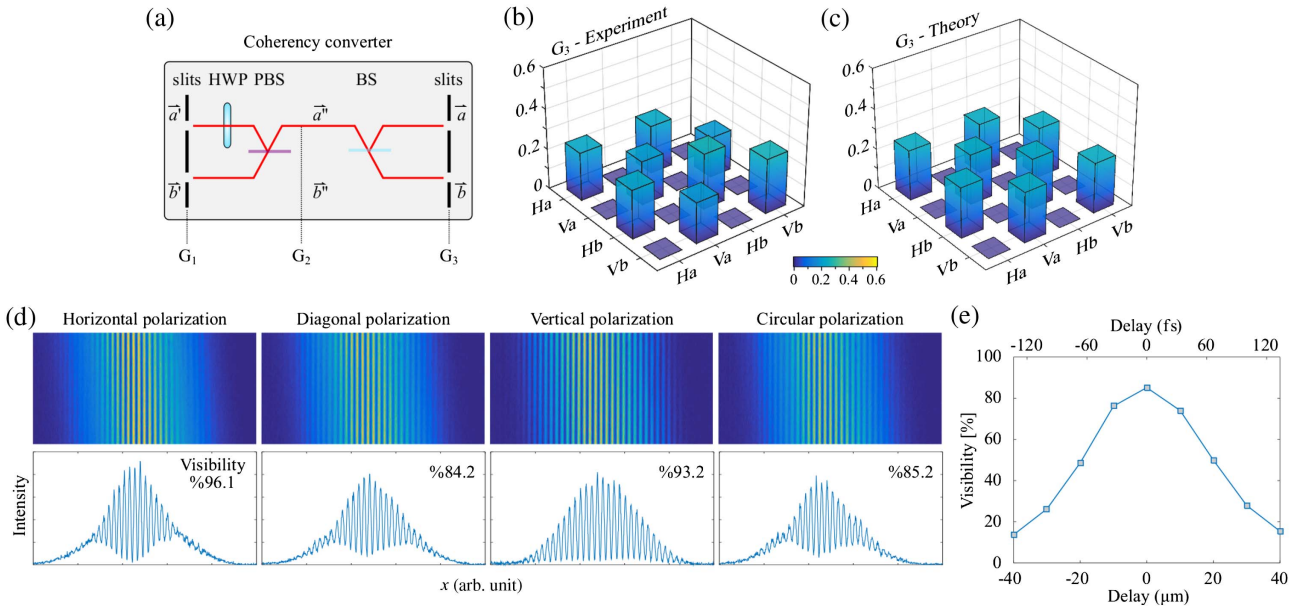

Fig. 5. (a) Schematic for the coherence converter that transforms two linearly polarized, spatially incoherent fields (at $\vec{a}'$ and $\vec{b}'$) into two randomly polarized mutually coherent fields (at $\vec{a}$ and $\vec{b}$). (b) Graphical depiction of the real part of the entries of the experimentally reconstructed $\boldsymbol{G}_3$ via OCmT. (c) The theoretical expectation for $\boldsymbol{G}_3$. (d) Interference patterns obtained by overlapping the fields from $\vec{a}$ and $\vec{b}$ after a polarization projection, with high-visibility fringes observed in all cases. The top panels are CCD camera images and the lower panels are obtained by integrating the fringes vertically. The main reasons for the different interference-fringe visibilities observed after the various polarization projections are experimental inaccuracies in aligning the two spatial modes and superposing them at the PBS and unequal slit sizes at $\vec{a}'$ and $\vec{b}'$. As a result, H and V projections display higher visibility than that for the diagonal and circular projections. (e) Visibility as a function of a relative delay inserted between the fields at $\vec{a}$ and $\vec{b}$ before overlapping them at the CCD camera [Fig. 2(c)] for the diagonal polarization projection case in (d).

Now that we have $G_{ab}^{\mathrm{HH}} + G_{ab}^{\mathrm{VV}} = \frac{1}{2}$, the predicted visibility is $V = 1$ [14]. Furthermore, because the two DoFs are independent *and* the field is unpolarized [as is clear from the separable form of $\boldsymbol{G}_3$ in Eq. (5)], projecting the polarization on any direction will not affect the high visibility [Fig. 5(d)]. Note that the coherence time of the field is determined by its spectral bandwidth, and observing the fringes [Fig. 5(d)] requires introducing a relative delay in the path of the fields from $\vec{a}$ or $\vec{b}$ before overlapping them [delay line 2 in Fig. 2(c)]. The variation in the measured visibility with introduced relative time delay corresponds to the expected field coherence time ≈100 fs (coherence length ≈30 μm) [Fig. 5(e)].

6. SURVIVING RANDOMIZATION THROUGH ENTROPY REALLOCATION

The ability to redistribute or reallocate the field entropy S between the DoFs can be exploited in protecting a DoF from the deleterious impact of a randomizing medium. Consider a depolarizing medium represented by a Mueller matrix $\hat{M} = \mathrm{diag}\{1, 0, 0, 0\}$ that converts *any* state of polarization into a completely unpolarized state. The initial field $\boldsymbol{G}_1$ [Figs. 3(b) and 3(c)] would be converted into the incoherent unpolarized field $\boldsymbol{G}_1' = \frac{1}{4}\mathrm{diag}\{1, 1, 1, 1\}$ upon traversing this medium with $S_{\mathrm{p}} \to 1$, such that $S \to 2$. If, however, coherence is first reversibly converted from the spatial DoF to polarization ($S_{\mathrm{p}} \to 1$ and $S_{\mathrm{s}} \to 0$), then traversing a depolarizing medium *cannot increase* S_{p}, and the field is thus left unchanged. Subsequently, the coherence conversion can be reversed and a polarized field is retrieved after emerging from the depolarizing medium without loss of energy.

We have carried out the proof-of-concept experiment depicted in Fig. 6(a) where we place a depolarizer or polarization scrambler in the path of the field $\boldsymbol{G}_2$ in the $(\vec{a}'', \vec{b}'')$ plane. The polarization

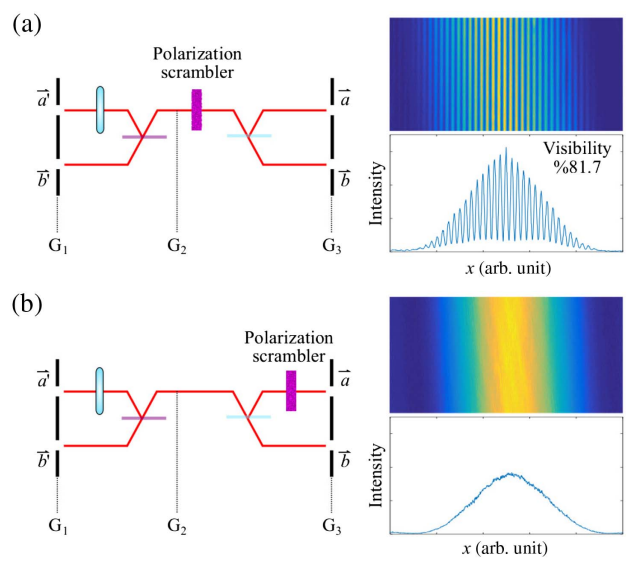

Fig. 6. Effect of a polarization scrambler on the field when introduced at two different planes. (a) A polarization scrambler is placed at the $\boldsymbol{G}_2$ plane (after the PBS at $\vec{a}''$) has no effect on the visibility of the interference pattern measured at the $\boldsymbol{G}_3$ plane, as shown in the right panels. (b) A polarization scrambler placed before $\vec{a}$ destroys the visibility. (a, b) The measurements in the right panels are averaged over the polarization shown in Fig. 5(d).

scrambler is implemented by rotating a HWP. The CCD camera exposure time is increased to 10 s, corresponding to the rotation time of the wave plate, to capture the averaged interference pattern in a single shot. The Mueller matrix associated with a polarization scrambler is $\hat{M} = \mathrm{diag}\{1, 0, 0, 0\}$. The visibility observed after the $(\vec{a}, \vec{b})$ plane remains high. This result can be modeled theoretically by first noting that a unitary transformation $\hat{U}$ transforms the field according to $\boldsymbol{G}_2 \to \boldsymbol{G}_2' = \hat{U}\boldsymbol{G}_2\hat{U}^\dagger$, where $\hat{U}$ is a 4×4 unitary transformation that spans the spatial and polarization DoFs. If the device in question impacts the two DoFs independently, then $\hat{U} = \hat{U}_\mathrm{s} \otimes \hat{U}_\mathrm{p}$, where $\hat{U}_\mathrm{s}$ and $\hat{U}_\mathrm{p}$ are 2×2 unitary transformations for the spatial and polarization DoFs, respectively. The impact of a randomizing but energy-conserving transformation can be modeled as a statistical ensemble of unitary transformations [27–29]. The transformation of $\boldsymbol{G}_2$ upon traversing a polarization scrambler can be expressed as

$$\boldsymbol{G}_2' = \sum_{j=1}^{4} p_j \{\hat{\mathbb{I}} \otimes \hat{U}_\mathrm{p}^{(j)}\}\boldsymbol{G}_2\{\hat{\mathbb{I}} \otimes \hat{U}_\mathrm{p}^{(j)\dagger}\}, \tag{6}$$

where $\hat{\mathbb{I}}$ is the 2×2 identity matrix and the ensemble $\{U_\mathrm{p}^{(j)}\}$ comprises with equal probabilities $p_j = \frac{1}{4}$ the Jones matrices: $\frac{1}{\sqrt{2}}\left(\begin{smallmatrix}1 & -1\\ 1 & 1\end{smallmatrix}\right)$, $\frac{1}{\sqrt{2}}\left(\begin{smallmatrix}1 & 1\\ 1 & -1\end{smallmatrix}\right)$, $\left(\begin{smallmatrix}1 & 0\\ 0 & -1\end{smallmatrix}\right)$, $\left(\begin{smallmatrix}0 & 1\\ 1 & 0\end{smallmatrix}\right)$, which correspond to polarization rotations of $\pm 45°$ in the H-V basis, and a HWP in the H-V basis and rotated by 45°. Substituting the ensemble $\{\hat{U}_\mathrm{p}^{(j)}\}$ into Eq. (6) yields $\boldsymbol{G}_2' = \boldsymbol{G}_2$, which entails that the high-visibility seen in Fig. 5(d) should be retained, as confirmed in Fig. 6(a). In other words, $\boldsymbol{G}_2$ is *invariant with regard to any polarization randomization*.

If the polarization scrambler is position dependent, the coherency matrix $\boldsymbol{G}_2$ will no longer be invariant under randomization (because the spatial and polarization DoFs become coupled). In the experiment illustrated in Fig. 6(b), the polarization scrambler is placed at $\vec{a}$ in the plane of $\boldsymbol{G}_3$. The spatial-polarization transformation of $\boldsymbol{G}_3$ takes the form

$$\begin{aligned}\boldsymbol{G}_3' = {} & \{\hat{\Lambda}_b \otimes \mathbb{I}\}\boldsymbol{G}_3\{\hat{\Lambda}_b^\dagger \otimes \mathbb{I}\} \\ & + \sum_{j=1}^{4} p_j \{\hat{\Lambda}_a \otimes \hat{U}_\mathrm{p}^{(j)}\}\boldsymbol{G}_3\{\hat{\Lambda}_a^\dagger \otimes \hat{U}_\mathrm{p}^{(j)\dagger}\},\end{aligned} \tag{7}$$

where we have $\hat{\Lambda}_a = \left(\begin{smallmatrix}1 & 0\\ 0 & 1\end{smallmatrix}\right)$ and $\hat{\Lambda}_b = \left(\begin{smallmatrix}0 & 0\\ 0 & 1\end{smallmatrix}\right)$, resulting in $\boldsymbol{G}_3' = \frac{1}{2}\hat{\mathbb{I}} \otimes \frac{1}{2}\hat{\mathbb{I}} = \frac{1}{4}\mathrm{diag}\{1, 1, 1, 1\}$; that is, an unpolarized and spatially incoherent field with maximal entropy $S = 2$ is produced. No fringes will appear in this case [Fig. 6(b)].

7. DISCUSSION AND CONCLUSION

To facilitate the analysis of the coherence of optical fields encompassing multiple DoFs, it is becoming increasingly clear that the mathematical formalism of multipartite quantum mechanical states is most useful [5,6,30]. The underlying foundation for this utility is the analogy between the mathematical descriptions used in these domains. The Hilbert space of a multipartite system is the tensor product of the Hilbert spaces of the single-particle subsystems. In classical optics, the multiple DoFs of a beam are described in a linear vector space having formally the structure of a tensor product of the linear vector spaces of the individual DoFs. In the quantum setting, pure multipartite states that cannot be separated into products of single-particle states are said to be entangled, whereas in the classical setting, fields in which the DoFs cannot be separated are now being called "classically entangled" [6]; coherence can be viewed as a "resource" that may be reversibly converted from one DoF of the beam to another, just as entanglement is a resource shared among multiple quantum particles. There is a critical difference though between the quantum and classical settings. Entanglement between initially separable particles requires nonlocal operations of particle–particle interactions (which are particularly challenging for photons [31]); on the other hand, entangling operations that couple different DoFs of a beam are readily available in classical optics. Adopting this information-driven standpoint has led to a host of novel opportunities and applications. For example, Bell's measure, originally developed for ascertaining nonlocality, becomes useful in quantifying the coherence of a multi-DoF beam and assessing the resources required to synthesize a beam of given characteristics [6]; beams in which spatial modes and polarization are classically entangled have been shown to enable fast particle tracking [32], local teleportation [33,34], and full Mueller characterization of a sample [35,36]; and introducing spatiotemporal spectral correlations leads to propagation-invariant pulsed optical beams [37,38].

We have demonstrated—for the first time to the best of our knowledge—the "conversion" or transformation of coherence from one DoF of an optical field to another, namely, from polarization to the spatial DoF. Starting from a field that is spatially incoherent but polarized, we redirect the statistical fluctuations from space toward polarization, resulting in an unpolarized field that is spatially coherent. Specifically, the 1 bit of entropy characterizing the spatial DoF was removed and added instead to the initially zero-entropy polarization. This is confirmed by multiple tests: (i) the field is found to be spatially coherent by reconstructing the 4×4 coherency matrix and observing the high-visibility interference fringes after overlapping the two field paths; (ii) the field is unpolarized as confirmed by the invariance of the outcome under different polarization projections; and (iii) the polarization and spatial DoFs are separable, as confirmed by repeating the spatial interference measurements and observing the invariance of the visibilities for all polarization projections. Entropy engineering of partially coherent optical fields can open the path to a variety of possible future extensions and applications with regard to optimizing the interaction of optical fields with disordered media.

Funding. Office of Naval Research (ONR) (N00014-14-1-0260, N00014-17-1-2458).

Acknowledgment. The authors thank A. Dogariu and D. N. Christodoulides for useful discussions.

†These authors contributed equally.

REFERENCES

1. L. Mandel and E. Wolf, *Optical Coherence and Quantum Optics* (Cambridge University, 1995).
2. F. Zernike, "The concept of degree of coherence and its application to optical problems," Physica **5**, 785–795 (1938).
3. M. Born and E. Wolf, *Principles of Optics*, 7th ed. (Cambridge University, 1999).
4. C. Brosseau, *Fundamentals of Polarized Light* (Wiley, 1998).
5. X.-F. Qian and J. H. Eberly, "Entanglement and classical polarization states," Opt. Lett. **36**, 4110–4112 (2011).
6. K. H. Kagalwala, G. Di Giuseppe, A. F. Abouraddy, and B. E. A. Saleh, "Bell's measure in classical optical coherence," Nat. Photonics **7**, 72–78 (2013).

7. A. F. Abouraddy, K. H. Kagalwala, and B. E. A. Saleh, "Two-point optical coherency matrix tomography," Opt. Lett. **39**, 2411–2414 (2014).
8. K. H. Kagalwala, H. E. Kondakci, A. F. Abouraddy, and B. E. A. Saleh, "Optical coherency matrix tomography," Sci. Rep. **5**, 15333 (2015).
9. E. Wolf, *Introduction to the Theory of Coherence and Polarization of Light* (Cambridge University, 2007).
10. A. Al-Qasimi, O. Korotkova, D. James, and E. Wolf, "Definitions of the degree of polarization of a light beam," Opt. Lett. **32**, 1015–1016 (2007).
11. A. F. Abouraddy, "What is the maximum attainable visibility by a partially coherent electromagnetic field in Young's double-slit interference?" Opt. Express **25**, 18320–18331 (2017).
12. C. Brosseau and A. Dogariu, "Symmetry properties and polarization descriptors for an arbitrary electromagnetic wavefield," in *Progress in Optics*, E. Wolf, ed. (Elsevier, 2006), Vol. **49**, Chap. 4, pp. 315–380.
13. F. Gori, M. Santarsiero, and R. Borghi, "Vector mode analysis of a Young interferometer," Opt. Lett. **31**, 858–860 (2006).
14. E. Wolf, "Unified theory of coherence and polarization of random electromagnetic beams," Phys. Lett. A **312**, 263–267 (2003).
15. J. Tervo, T. Setälä, and A. T. Friberg, "Degree of coherence of electromagnetic fields," Opt. Express **11**, 1137–1143 (2003).
16. T. Setälä, J. Tervo, and A. T. Friberg, "Complete electromagnetic coherence in the space-frequency domain," Opt. Lett. **29**, 328–330 (2004).
17. F. Gori, M. Santarsiero, and R. Borghi, "Maximizing Young's fringe visibility through reversible optical transformations," Opt. Lett. **32**, 588–590 (2007).
18. R. Martínez-Herrero and P. M. Mejías, "Maximum visibility under unitary transformations in two-pinhole interference for electromagnetic fields," Opt. Lett. **32**, 1471–1473 (2007).
19. A. Peres, *Quantum Theory: Concepts and Methods* (Kluwer Academic, 1995).
20. W. K. Wootters, "Local accessibility of quantum states," in *Complexity, Entropy, and the Physics of Information*, W. H. Zurek, ed., Vol. **VIII** of SFI Studies in the Sciences of Complexity (Addison-Wesley, 1990), pp. 39–46.
21. D. F. V. James, P. G. Kwiat, W. J. Munro, and A. G. White, "Measurement of qubits," Phys. Rev. A **64**, 052312 (2001).
22. A. F. Abouraddy, A. V. Sergienko, B. E. A. Saleh, and M. C. Teich, "Quantum entanglement and the two-photon Stokes parameters," Opt. Commun. **201**, 93–98 (2002).
23. F. Gori, "Matrix treatment for partially polarized, partially coherent beams," Opt. Lett. **23**, 241–243 (1998).
24. J. Ellis and A. Dogariu, "Complex degree of mutual polarization," Opt. Lett. **29**, 536–538 (2004).
25. M. Mujat, A. Dogariu, and E. Wolf, "A law of interference of electromagnetic beams of any state of coherence and polarization and the Fresnel–Arago interference laws," J. Opt. Soc. Am. A **21**, 2414–2417 (2004).
26. A. Aiello, F. Toppel, C. Marquardt, E. Giacobino, and G. Leuchs, "Quantum-like nonseparable structures in optical beams," New J. Phys. **17**, 043024 (2015).
27. K. Kim, L. Mandel, and E. Wolf, "Relationship between Jones and Mueller matrices for random media," J. Opt. Soc. Am. A **4**, 433–437 (1987).
28. J. J. Gil, "Characteristic properties of Mueller matrices," J. Opt. Soc. Am. A **17**, 328–334 (2000).
29. O. Gamel and D. F. V. James, "Causality and complete positivity of classical polarization maps," Opt. Lett. **36**, 2821–2823 (2011).
30. B. N. Simon, S. Simon, F. Gori, M. Santarsiero, R. Borghi, N. Mukunda, and R. Simon, "Nonquantum entanglement resolves a basic issue in polarization optics," Phys. Rev. Lett. **104**, 023901 (2010).
31. V. Venkataraman, K. Saha, and A. L. Gaeta, "Phase modulation at the few-photon level for weak-nonlinearity-based quantum computing," Nat. Photonics **7**, 138–141 (2013).
32. S. Berg-Johansen, F. Töppel, B. Stiller, P. Banzer, M. Ornigotti, E. Giacobino, G. Leuchs, A. Aiello, and C. Marquardt, "Classically entangled optical beams for high-speed kinematic sensing," Optica **2**, 864–868 (2015).
33. S. M. Hashemi Rafsanjani, M. Mirhosseini, O. S. Magana-Loaiza, and R. W. Boyd, "State transfer based on classical nonseparability," Phys. Rev. A **92**, 023827 (2015).
34. D. Guzman-Silva, R. Brüning, F. Zimmermann, C. Vetter, M. Grafe, M. Heinrich, S. Nolte, M. Duparre, A. Aiello, M. Ornigotti, and A. Szameit, "Demonstration of local teleportation using classical entanglement," Laser Photon. Rev. **10**, 317–321 (2016).
35. F. Töppel, A. Aiello, C. Marquardt, E. Giacobino, and G. Leuchs, "Classical entanglement in polarization metrology," New J. Phys. **16**, 073019 (2014).
36. S. Tripathi and K. C. Toussaint, "Rapid Mueller matrix polarimetry based on parallelized polarization state generation and detection," Opt. Express **17**, 21396–21407 (2009).
37. H. E. Kondakci and A. F. Abouraddy, "Diffraction-free pulsed optical beams via space-time correlations," Opt. Express **24**, 28659–28668 (2016).
38. K. J. Parker and M. A. Alonso, "Longitudinal ISO-phase condition and needle pulses," Opt. Express **24**, 28669–28677 (2016).